Transp Porous Med (2012) 94:537–554
DOI 10.1007/s11242-012-0017-x

Connectivity of Pore Space as a Control on Two-Phase Flow Properties of Tight-Gas Sandstones

Maryam A. Mousavi · Steven L. Bryant

Received: 1 November 2011 / Accepted: 19 April 2012 / Published online: 4 May 2012

Abstract We predict capillary-pressure (drainage) curves in tight-gas sandstones which have little matrix or microporosity using a quantitative grain-scale model. The model accounts for the geometric results of some depositional and diagenetic processes important for porosity and permeability reduction in tight-gas sandstones, such as deformation of ductile grains during burial and quartz cementation. The model represents the original sediment as a dense, disordered packing of spheres. We simulated the evolution of this model sediment into a low-porosity sandstone by applying different amounts of ductile grains and quartz precipitation. A substantial fraction of original pore throats in the sediment is closed by the simulated diagenetic alteration. Because the percolation threshold corresponds to closure of half of the pore throats, the pore space in this type of tight-gas sandstone is poorly connected and is often close to being completely disconnected. The drainage curve for different model rocks was computed using invasion percolation in a network taken directly from the grain-scale geometry and topology of the model. Some general trends follow classical expectations and were confirmed by experimental measurements: increasing the amount of cement shifts the drainage curve to larger pressures. This is related to reduction of the connectivity of pore space resulting from closure of throats. Existence of ductile grains in the ductile grain model also reduces the connectivity of pore space but it treats the throats distribution differently causing the drainage curves to be shifted to larger irreducible water saturation when cement is added to the model. The range of porosities in which these connectivity effects are important corresponds to the range of porosities common for tight gas sandstones. Consequently these rocks can exhibit small effective permeability to gas even at large gas saturations. This problem

This article was previously presented in AAPG Annual Convention and Exhibition, June 7–10, Denver, Colorado, 2009.

M. A. Mousavi (✉)
Bureau of Economic Geology, The University of Texas at Austin, 10100 Burnet Rd.,
Austin, TX 78758, USA
e-mail: maryam.s.mousavi@gmail.com

S. L. Bryant
Petroleum and Geosystems Engineering, The University of Texas at Austin,
1 University Station C0300, Austin, TX 78712-0228, USA

occurs at larger porosities in rocks with significant content of ductile grains because ductile deformation blocks a significant fraction of pore throats even before cementation begins. Predicted drainage curves agree with measurements on two samples with little microporosity, one dominated by rigid grains, the other containing a significant fraction of ductile grains. We conclude that connectivity of the matrix pore space is an important factor for an understanding of flow properties of tight-gas sandstones.

Keywords Connectivity of pore space · Tight gas sandstone · Drainage curve · Percolation threshold · Blocked throats

1 Introduction

Unconventional natural-gas resources, particularly tight-gas sands, constitute a significant percentage of the natural-gas resource base and offer abundant potential for future reserves and production. Unlike conventional oil and gas reservoirs, tight-gas sands have unique gas-storage and producing characteristics that can be attributed to postdepositional diagenetic processes, including mechanical compaction, quartz and other mineral cementation, grain replacement, and mineral dissolution. These processes lead to permanent alteration of the initial pore structure, causing an increase in tortuosity and a subsequent increase in number of isolated and disconnected pores. The resulting tight-gas sandstone will have low gas storage because of the small pore system.

Gas productivity in tight-gas sandstone reservoirs is controlled by geological attributes. According to the study of Dutton et al. (1993), most tight-gas formations in the United States are well-sorted sandstones deposited in high-energy depositional systems, which contain large amounts of authigenic, intergranular cement, and are not, in general, muddy sandstones with abundant detrital clay. Production characteristics of low-permeability reserves are controlled largely by diagenesis. Important parameters, which alter the diagenetic process, are sediment composition, depth of burial, and age of the reservoir. Other geological attributes critical to gas production of tight-gas sandstones are natural fractures and stress direction. Knowledge of natural fractures benefits design of completion and stimulation practices and guides drilling strategies (Dutton et al. 1993).

Capillary-pressure data are useful in evaluating the producibility of tight-gas sandstones. Even at extremely high capillary pressure, a large amount of water will be preserved because of surface adsorption and capillary condensation. Producibility of the tight sandstone diminishes at high water saturation, similar to producibility of conventional rocks because the relative permeability of gas is greatly reduced. Thus, water forced into a low-permeability reservoir during drilling or fracture stimulation is slow to flow back to the well (clean up). This water may never return to the well from a very tight reservoir, preventing the reservoir from regaining its original permeability (Dutton et al. 1993).

The effect of pore throat size on capillary pressure curves is familiar and is the primary influence on two-phase properties in conventional rocks. Throat size remains a first-order influence in low-porosity rocks, but the closure of pore throats by cementation has a comparable influence when porosity drops below 10 %. For example, the exponent n in a power-law trend of permeability against porosity $\kappa/\kappa_0 = (\phi/\phi_0)^n$ in clean, well sorted sandstone changes from $n \sim 3$ for porosities greater than 15 % to $n \sim 7$ for porosities less than 10 % (Bourbie and Zinszner 1985). This change can be explained by the reduction in overall connectivity of pore space (Bryant et al. 1993). Consequently in tight gas sandstones, which

generally exhibit porosities less than 10 % and often as small as 5 %, we anticipate a strong influence of pore space connectivity on the properties of these rocks.

Drainage is fundamentally a percolation process, and percolation depends strongly upon lattice connectivity. The goal of this paper is to model pore-scale geometry and capillary pressure curves for a better understanding of the connectivity of pore space in these rocks, which, in turn, will lead to a better understanding of their reservoir behavior. In this paper, we restrict the modeling to rocks with primarily intergranular porosity. Rocks with substantial matrix porosity (detrital silt or clay that fills intergranular volume between framework grains) or microporosity (e.g., in altered feldspars) require more complicated pore space models (Mehmani et al. 2011).

Direct measurement of the 3D void space in tight gas sandstones is not routine. On one hand it requires resolving voids smaller than 1 micron and often smaller than 0.1 micron. On the other, assessing the connectivity of these voids requires a large sample volume. Methods that could meet these requirements are being actively investigated. Pending the availability of suitable datasets, here we adapt a geometric modeling technique that has proven useful for conventional clastics. The main assumptions of the model are (i) the precursor sediment is a dense, disordered packing of spheres; (ii) deposition of cement corresponds to increasing the radii of the spheres without moving their centers; (iii) compaction corresponds to moving sphere centers closer to each other in one direction; (iv) deformation of ductile grains corresponds to interpenetration of spheres; (v) the capillary entry pressure of a pore throat is inversely proportional to the radius of a circle inscribed in that throat. To simplify the presentation, in this paper we consider only monodisperse packings and apply cement uniformly to all grains. These restrictions are not essential; Mousavi (2010) illustrate the behavior for polydisperse packings and nonuniform cementation.

2 Models of Granular and Consolidated Material

The central obstacle to quantitatively and predictively relating microscopic structure of sedimentary rocks to their macroscopic properties has been the difficulty in characterizing pore space. One way of characterizing the pore space in a granular material is to construct a close, disordered packing of equal spheres. Finney (1968) constructed such a packing, which consisted of 25,000 ball bearings confined by a rubber bladder and fixed by means of waxes. Finney measured the spatial coordinates of the centers of some 8,000 spheres in the core of this packing (by special machines), to determine both solid and void space within the packing. Mason (1972) showed that Finney's measurement of grain locations in a dense, disordered packing of equal spheres could be used to extract pore-throat sizes, which, in turn, could be used to estimate capillary-pressure curves (phase volume fraction versus applied capillary pressure) in an unconsolidated granular material. An alternative to measuring grain location would be to simulate the packing process on a computer.

Much of the predictive power of sphere pack models stems from the disorder of location of grains. Such models enable remarkably accurate predictions of macroscopic properties of rocks as a function of the extent of various geological processes, such as quartz cementation. For example, Roberts and Schwartz (1985) used Finney's data to estimate electrical conductivity in the packing of nonconducting grains filled with a conducting fluid. Bryant et al. (1993) adapted the approach of Mellor (1989) to predict permeability in sandstones. Starting with the original Finney packing, porosity was reduced by increasing the radius of the spheres without changing the sphere locations, thus modeling the growth of quartz cement. Increasing all radii uniformly provided an accurate a

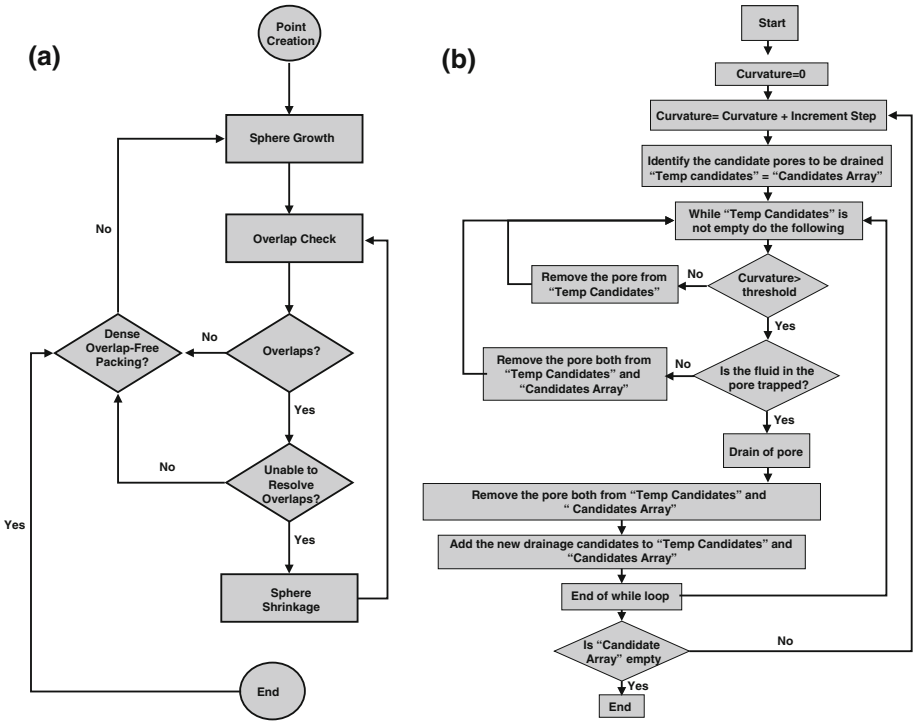

Fig. 1 **a** *Flowchart* for cooperative rearrangement algorithm without ductile grains (figure courtesy from Thane 2006). **b** Drainage model simulation flowchart (figure courtesy from Behseresht 2008)

priori prediction of the permeability/porosity trend of well-sorted, quartz-cemented sandstones (Bryant et al. 1993). The key advantage of this model is that geometry of the pore space in the model rocks is completely determined because the grain space is completely determined; all sphere locations are known, as are their radii. Others have since used sphere packing to model transport properties of porous media. Mason and Mellor (1995) used Finney packing data after converting a network model to simulate drainage and imbibition in a porous medium. Sphere packing has also been used to model compaction and cementation of a conventional sandstone (e.g., Jin et al. 2006). Here, we extend these concepts to model tight-gas sandstones with low porosity and permeability due to extensive deformation of ductile grains during compaction and cementation. The model of compaction is a simple rescaling of one coordinate axis, which has the effect of moving the spheres closer together causing some to overlap. The model of the deformation of grains during compaction is adapted from the approach of Thane (2006) who accounted for the geometric change in lithic grains using a soft-shell (penetrable sphere) model (Fig. 1). The cooperative rearrangement algorithm with soft-shell grains provides reasonable prediction of the porosity of compacted mixtures of ductile and rigid grains (Mousavi and Bryant 2007, 2011; Mousavi 2010). In addition, cementation can be modeled by simply adding to each grain like an onion skin to account for overgrowth rim cementation in sandstones. For a given geometrical set of parameters, many realizations for sphere packing can be generated. Although each realization differs in detail, but average properties such as connectivity are remarkably consistent between realizations (Thane 2006).

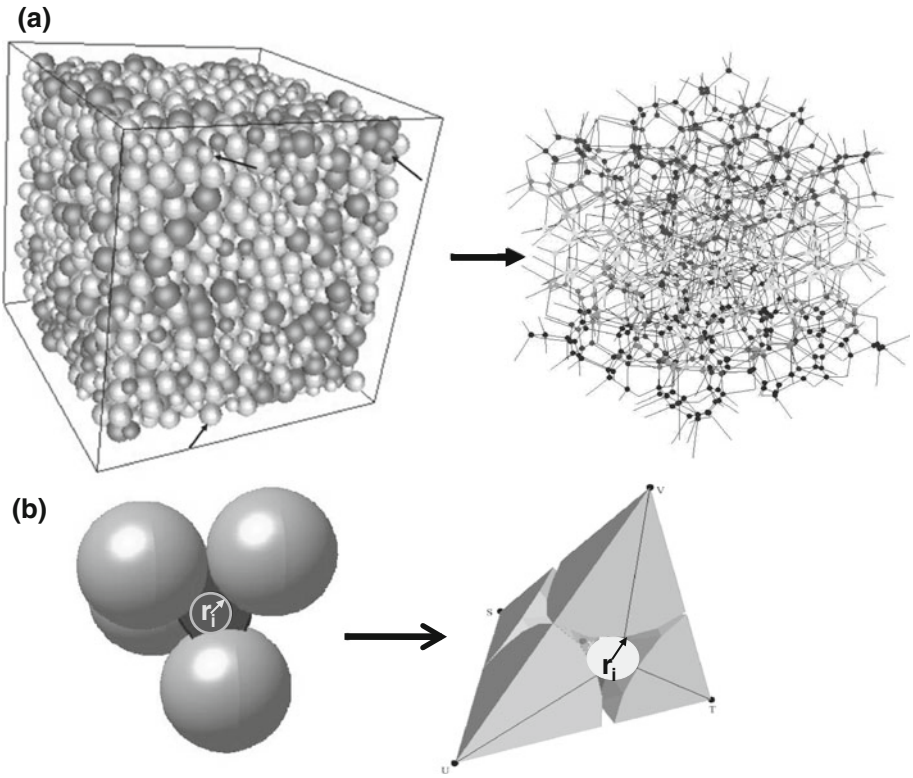

Fig. 2 **a** From the model sandstone (*left*) we extracted a network model of pore space (*right*), which is an easy and effective tool for determining flow properties of the model rock. The network model represents pore space as a *graph* of interconnected sites. Nodes of the graph represent pore bodies, whereas the *lines* connecting the nodes indicate pore throats, which connect pore bodies to flow. **b** Delaunay tessellation is a tool for identifying pores and throats in the model rock. Delaunay tessellation finds the nearest neighbor spheres in the packing and groups them in a tetrahedron. A pore body is the empty space between four spheres in a tetrahedron, and a pore throat is the empty space between the three spheres of each face. These data will be used to build a network model. The radius of a *circle* inscribed in a pore throat is denoted r_i

The grain-scale model is an input for network modeling (Fig. 2a). We first analyze the topology and geometry of the pore space from the grain-scale model.

We find pore-body and pore-throat information location by grouping grains into nearest-neighbor clusters (Delaunay tetrahedron) (Fig. 2b). This method allows identification of pore and throat blocking during compaction and cementation. This provides a prediction of connectivity of pore space as a function of the extent of porosity-reducing processes. The prediction can be tested indirectly against measurements of other rock properties that depend on connectivity (Mousavi 2010). Other approaches for obtaining network geometry can be found in Valvatne and Blunt (2004), Al-Raoush et al. (2003), and Joekar-Niasar et al. (2010).

3 Modeling of Ductile Grains and Their Deformation

To model a ductile grain (lithic grain) we used a soft-shell model sphere, in which grains can interpenetrate until their inner rigid cores come into contact (Thane 2006; Mousavi and Bryant 2007, 2011; Mousavi 2010). We varied the fraction of grains assumed ductile and

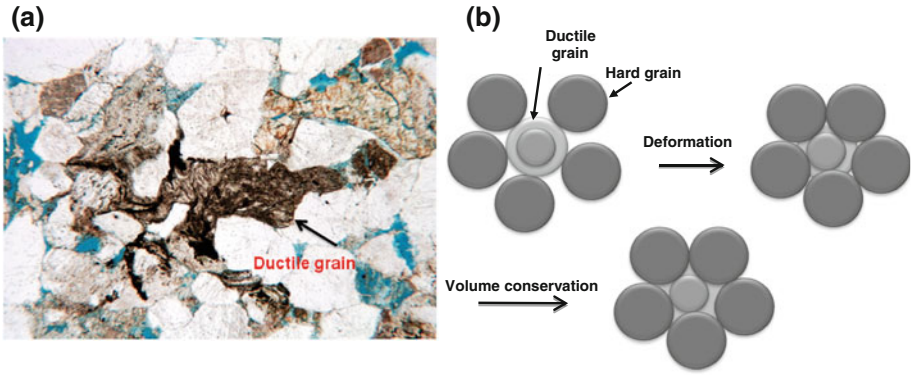

Fig. 3 **a** Ductile deformation of mica-rich lithic grains; Pennsylvanian Breathitt Sandstone, S. Appalachian Basin (Milliken et al. 2007). This is a fine grain sandstone. **b** Schematic of one ductile grain pressing into five hard grains. Overlap stops when hard grain reaches rigid core of ductile grain. Volume conservation calculated at the end and added to outer shell of ductile grain. The ductile grain fills the pore space between grains in a way similar to the plastic flow of ductile grains into pore space between rigid grains, as in (**a**)

the radii of the rigid cores of the ductile grains. The radius of the rigid core is a proxy for ductility of grains, and by increasing this rigid core, we decreased the ductility of the grain. The overlap of the grains represents the pressing of ductile grains into other grains as a result of compaction (Fig. 3a). Then we calculated the amount of overlap and added to the outer shell of the ductile grain to account for mass conservation (Thane 2006; Mousavi 2010). Figure 3b is a schematic of one ductile grain (lithic) pressing into five hard (quartz) grains. A complete explanation of this model can be found in recent literature (Mousavi and Bryant 2007, 2011; Mousavi 2010).

4 Cementation Model

Because cementation introduces minerals into the pore system of the rock, it does not reduce the bulk volume of the rock. In sandstone overgrowth, quartz cementation is the most common cement (Worden and Morad 2000). Houseknecht (1984) concludes that more intergranular pressure solution occurs in finer grained sandstones than in coarser grained rocks. This leads to less minus-cement porosity in the finer grained sandstones. He also observes that some of the pressure-dissolved quartz is exported from the finer-grained sandstone, while the coarser grained sandstone imports quartz cement.

We can model this situation as follows. First, we account for the burial with pressure solution. Bryant et al. (1993) showed that the permeability/porosity trend for a simple model of pressure dissolution was the same as the trend for quartz overgrowth cementation, even though the details of the pore geometry were affected differently by each mechanism. Thus, for the purposes of estimating average pore space properties, we can represent the burial-induced pressure solution by a suitable thickness of overgrowth cement. This thickness on fine grains is a greater fraction of the grain radius than on coarse grains, because the finer grains undergo more pressure dissolution.

The second step is to account for the export of pressure-dissolved material from the finer grained regions and import of material into the coarser grained regions. Houseknecht (1984) concludes that more intergranular pressure solution occurs in finer grained sandstones than in coarser grained rocks, and that pressure-dissolved quartz is exported from the finer-grained sandstone, while the coarser grained sandstone imports quartz cement. We do this by reduc-

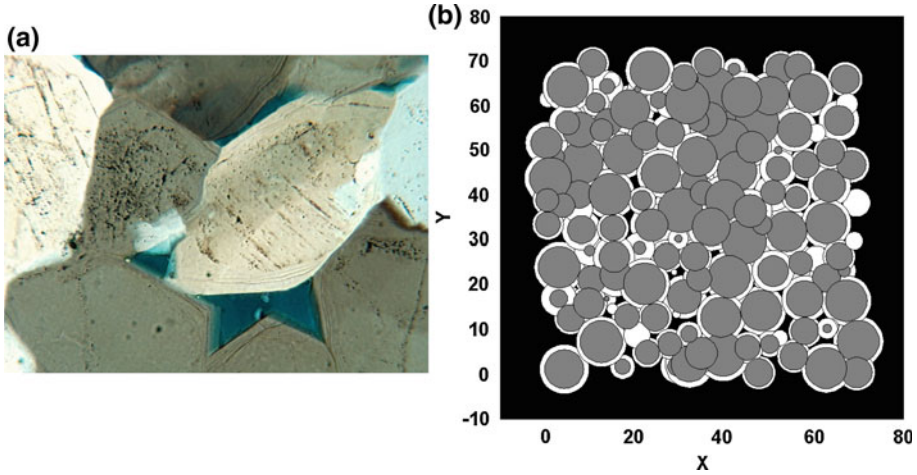

Fig. 4 **a** Overgrowth quartz cementation (Milliken et al. 2007). This is a fine grain sandstone. **b** 2D thin section of dense random packing of 1,000 spheres in bidispersed packing (radius ratio of 1.5 and 50 % *small spheres*), with 30 % ductile spheres (having 0.7 rigid radius). We grew $0.2r_i$ overgrowth cement on the grains and reduced porosity to 7 %. The original porosity in this packing was 22 %. Differences in grain radii in the 2D section are related to bidispersed grains sizes and position of the section relative to grain centers. *Gray* grains (*spheres*), *white* overgrowth cement

ing the thickness of cement on the smaller grains and increasing the thickness on the larger grains Mousavi and Bryant (2011). The net effect is to make the ratio of cement thickness to grain radius more similar on the fine and the coarse grains. It is convenient to work with the special case of having the same thickness/radius ratio for all grains, and we take this case to represent the overall influence grain size distribution on intergranular pressure solution plus export and import of cement.

Thus to model overgrowth cement, we increased radii of spheres in a model sediment without changing the position of the sphere centers. That is, the cement thickness ΔR_i on the ith grain is given by $\Delta R_i = aR_i$ where a is a constant. Thus, larger spheres have thicker overgrowth cement in absolute terms. Figure 4 shows overgrowth cementation in a sandstone and in one of the model rocks with ductile grains (Fig. 4b). The porosity of the model rock decreased from 22 to 7 % by addition of $0.2r_i$ (i.e., $a = 0.2$) cement to all grain.

5 Drainage Simulation

To calculate drainage in the network representation of pore space in the model tight gas sandstones, we used methods of Behseresht (2008) and his code in Matlab®. The method has been elaborated by Mason and Mellor (1995), Bryant et al. (1993, 1996), Gladkikh and Bryant (2005), Behseresht et al. (2008, 2009), Behseresht and Bryant (2011) and Mousavi (2010). A brief explanation of the method follows.

To obtain a network of pores and throats from a grain-scale model we use a tool to convert the grain-scale data (radii and center of spheres) to void space of bonds and sites in a network model (bonds represent pore throats, and sites represent pore spaces of a real rock). The tool is a Delaunay tessellation routine, which finds the nearest neighbor points in a set of points. A group of nearest-neighbor points forms a tetrahedron. Each tetrahedron corresponds to

four spheres containing void space, which we call *pore space* or *porosity*. Each face of the tetrahedron has three spheres with an open space in between, which we call a *pore throat*. In other words, each tetrahedron has one pore and four pore throats (Fig. 2b). When all pores are open, connectivity = 4.

We quantify the pore space between spheres by considering a sphere inscribed between four spheres in each Delaunay tetrahedron. We quantify a pore throat by a circle inscribed between three spheres in each face of the Delaunay tetrahedron. The radii of the circles in the throats are called *inscribed radii*, which have a crucial role in simulation of single- and multi-phase flow.

To simulate capillary displacement of the wetting phase by a nonwetting phase in the network model, the critical drainage curvature of each throat is computed. The critical curvature is the smallest curvature for which the meniscus between nonwetting and wetting phase can pass through a throat. To estimate this drainage curvature we use the Haines criterion (insphere approximation) (Haines 1930) with a Mason and Mellor (1995) modification, which subtracts 1.6 from the Haines criterion:

$$C = \frac{2}{r_{\text{inscribed}}} - 1.6 \tag{1}$$

where $r_{\text{inscribed}}$ is the inscribed radius.

We model drainage as constrained invasion percolation, where the constraint is that the displacement of wetting phase from the network must be explicitly accounted for. The method amounts to a set of rules to determine which candidates for drainage are invaded by the nonwetting phase. A pore containing wetting phase and having at least one neighbor pore empty of the wetting phase is a candidate for drainage. This candidate will be drained only if both the following conditions are satisfied: (i) the applied curvature exceeds the critical curvature of the throats connecting this pore and its neighbor, and (ii) there is a connected path of wetting phase between this pore and the outlet of the network.

Following Behseresht (2008), we consider pendular rings and liquid bridges when determining the connectivity of the wetting phase. The pendular ring is a volume of the wetting phase between two grains that are in point contact. Liquid bridges are bridges of the wetting phase between two grains having a small gap between them. Liquid bridges disappear when drainage exceeds threshold drainage for that specific throat, whereas pendular rings are always there, regardless of drainage (Fisher 1962; Gladkikh and Bryant 2005; Behseresht 2008; Behseresht et al. 2008, 2009; Behseresht and Bryant 2011).

The simulation starts with a few pores on one face of the packing in contact with the nonwetting phase, and the applied curvature is increased in small increments. In each increment, all of the pores in the path from the source, which meet the criteria described above, will be invaded until no more candidates can be found. Drainage will be complete when none of the remaining wetting phase is connected to the outlet of the packing. The simulated drainage curves are plotted in terms of dimensionless curvature, which is equivalent to dimensionless capillary pressure and is defined as:

$$C = \frac{P_c \times R_{\text{mean}}}{\sigma} \tag{2}$$

where C is dimensionless drainage curvature, P_c is drainage capillary pressure, R_{mean} is average grain radii before cement or compaction, and σ is the interfacial tension between gas and water (or wetting and nonwetting fluids used in the experimental data).

6 Drainage Simulation in Poorly Connected Rocks

Drainage curves have been calculated as described above for a variety of models of rock (Mousavi 2010). Grain size distribution does not change the drainage curve except when we have a much skewed distribution with high standard deviation (Behseresht 2008); therefore we modeled our samples with monodispersed packings. First, we added only cement to all of the grains in monodispersed packing. Different amounts (thicknesses) of cement were added uniformly to all grains after the monodispersed packing had been made. In other words, we held the center of grains fixed and then increased the radii of grains uniformly by a certain amount. The set of models represents extremely well sorted sandstone with a wide range of porosities. Figure 5 shows the drainage curves for this set of model rocks. Increasing the amount of cement causes the drainage curve to shift upwards for packings with small porosities below 10 %. The drainage curves for porosities greater than 10 % have very similar shape, as should be expected since the effect of cement in this range of porosity is simply to reduce all pore throat radii together. For porosity less than 10 %, drainage requires a steady increase in curvature to displace wetting phase, i.e., $dP_c/dS_w < 0$ after the capillary pressure exceeds the entry pressure. As porosity decreases, the magnitude of dP_c/dS_w increases. The percolation phenomenon, when a small increase in curvature displaces a large volume of wetting phase, i.e., $dP_c/dS_w \approx 0$, no longer occurs. This is a manifestation of the decrease in pore connectivity as additional cement closes pore throats. The explanation of this phenomenon lies in the pore scale geometry in the different packings, which we discuss in the next section.

Figure 6 shows the drainage curves for the model rocks with significant ductile grain content (40 % ductile matter in the model sediment, rigid radius of ductile grains = 0.7) and different degrees of cementation. Compaction of the ductile grains results in a porosity of 17 %. After compaction, the addition of different thicknesses of cement on the rigid grains yields a second set of model rocks. The low porosity models correspond to tight-gas sandstones which have little microporosity. In these models, the effect of cement is even more pronounced than in Fig. 5. The deformed ductile grains have blocked a fraction of pore throats even before cementation starts. Adding cement causes the irreducible water saturation to increase significantly as the pore space connectivity decreases. By addition of $0.22r_i$

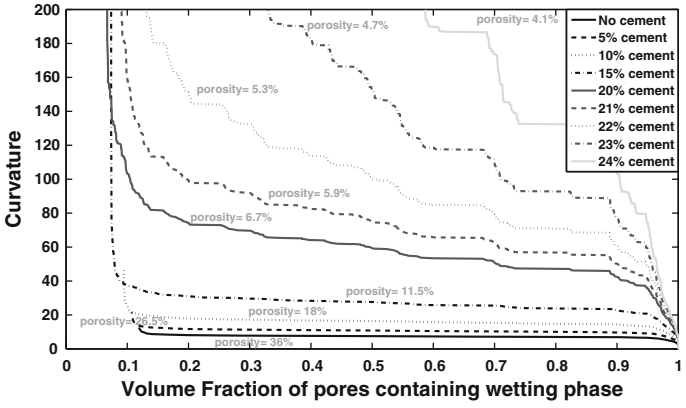

Fig. 5 Drainage curves for very well sorted, rigid-grain dominated model rocks with different amounts of cement. Curvature is dimensionless capillary pressure. All of packings contain 5,000 spheres

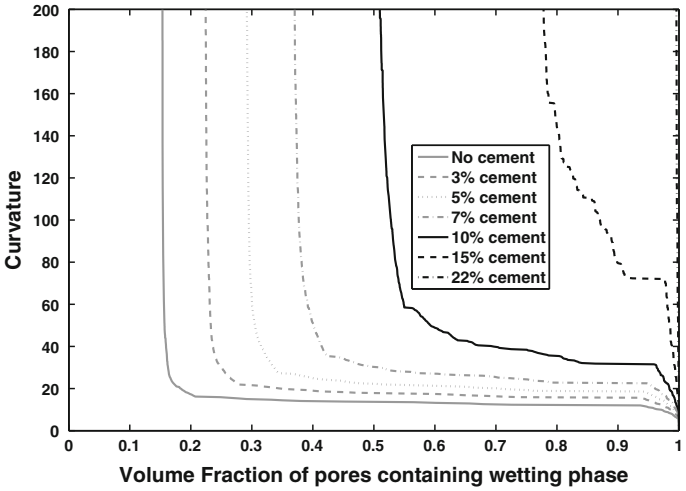

Fig. 6 Drainage curves for very well sorted model rocks with 40 % ductiles by volume in the original sediment, 0.7 rigid radii of ductile grains, and different cementation (different % of sphere radius). Curvature is dimensionless capillary pressure. Packings contain 5,000 spheres

cement (22 % of sphere radius), nearly all the pores are isolated and the drainage curve shifts to the extreme right side of the plot. In contrast in the case of cement in a packing without ductile grains (Fig. 5), even the addition of $0.24r_i$ cement (24 % of rigid radii of sphere) left many of the pores still connected. Connectivity and the percolation threshold will be examined in detail in the section that follows.

7 Connectivity of Pore Space

The distribution of sizes of open pore throats and the fraction of closed pore throats can be obtained from the Delaunay tessellation of each model rock. Average connectivity of pore space is the number of open throats in each pore in the packing. Average connectivity of pore space is equal to four for a monodispersed packing of spheres, such as Finney's packing with 36 % porosity, because all four throats in each pore are open. If cementation and ductile deformation have closed some of the pore space and related pore throats in rocks, the average connectivity must be less than four.

The histogram of number of open throats in each pore is shown in Fig. 7 for model rocks with a wide range of cement formed from a sediment without ductile grains. No pores have blocked throats when the cement thickness is less than $0.15r_i$. When the cement thickness is $0.15r_i$, nearly 20 % of the pores have one blocked throats, and 5 % have two blocked throats. Subsequent increments in cement thickness steadily reduce the number of pores that still have four open throats, and the fraction of pores with two closed throats increases rapidly. A few pores have three or four closed throats.

The histograms of Fig. 7 can be summarized in terms of the average pore connectivity as shown in Fig. 8a. Cementation does not affect connectivity until the cement thickness exceeds $0.1r_i$. The connectivity decreases linearly for greater cement thickness. The reduction may not seem dramatic in terms of the numerical values; the "average pore" has 3.2 open throats when the cement thickness is $0.24r_i$ and the porosity is only 4.1 %. The fraction of blocked

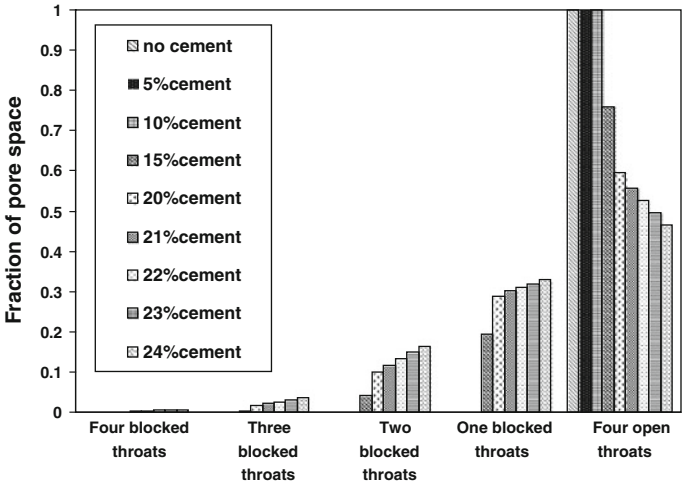

Fig. 7 Fraction of pores of different blocked-throat status for rigid-grain model rocks. When cement is added to the packing, the fraction of pores with four open throats gets smaller, and the fraction of pores with at least one blocked throat increases. Percentage of cement corresponds to the value of a, which determines cement thickness as a linear function of grain size (see text)

throats may (Fig. 8b) be a more sensitive measure of how the reduced connectivity can affect fluid movement: at the same cement thickness of $0.24r_i$ 40 % of the pore throats are blocked. This is close to the percolation threshold for this type of lattice (Bryant et al. 1993).

The drainage simulations for this series of model rocks (Fig. 5) show that when connectivity of pore space is decreased (increasing cement above $0.15r_i$ thickness), the drainage curve shifts upward and toward the right. When the connectivity is not changing (cement less than 15 % thickness), the drainage curves shift only upward. The width of the size distribution for open pore throats increases with each increment of cement thickness, as shown in Fig. 9. All else being equal, a wider throat size distribution will shift the drainage curve upwards, but it will not change the shape of the drainage curve: the network will still percolate when the threshold is reached. Thus, the behavior of the drainage curves in Fig. 5 is primarily due to the connectivity variation and not to the variation in pore throat size distribution. We expand on this point in the next section.

Figures 8 and 10 show the connectivity statistics for the model compacted sediment containing 40 % ductile grains with a range of thicknesses of overgrowth cement. For the same thickness of cement, these model rocks have smaller average connectivity than the models without ductile grains. This is because the compaction process has already blocked a significant fraction of pore throats (about 15 %) with ductile material deformed from its original location in the uncompacted sediment (Fig. 8b). Increasing the amount of cement in the compacted model sediment decreases the average connectivity of the pore space at about the same rate as when only rigid grains are present. The distributions of sizes of open pore throats are much wider than the distributions for the rigid-grain model rocks. The greater width is because some throats are not quite closed by the deformed ductile material. This is an important difference, because the growth of only a little cement on the rigid grains in those not-quite-closed throats will close them. However, in throats formed by only rigid grains, the same amount of cement reduces the throat sizes by a small, uniform amount. This is evident in the similar shape of the pore throat size distributions for throat radii greater than 10^{-1}

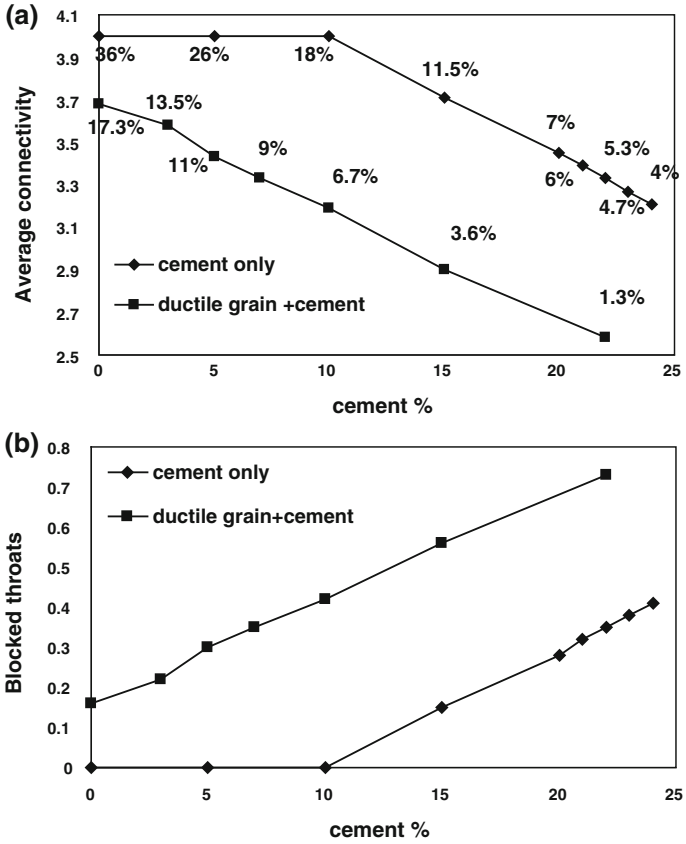

Fig. 8 **a** Average connectivity of pore space for both rigid and ductile grain (40 % of grains are ductile with 0.7 rigid radii) models. Increasing cement decreases connectivity of pore space. Percentage on top of data show the porosity percentage for each packing. **b** Fraction of blocked throats versus cementation. With the addition of more cement, more throats close. Values Percentage of cement = different percentages of sphere radii added to sphere radii

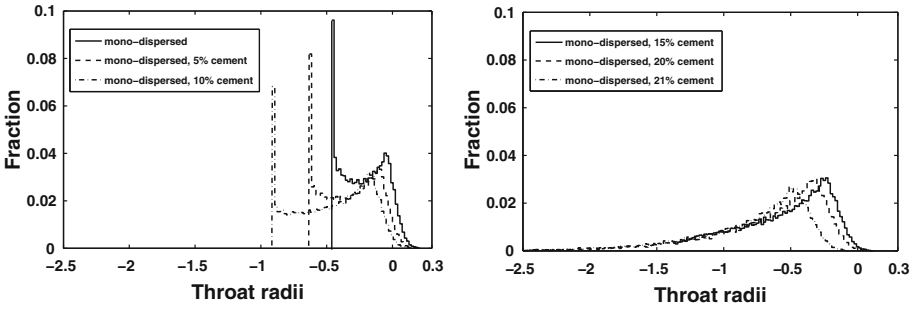

Fig. 9 Throat-size distribution (inscribed radii, logarithm values) for rigid-grain model rocks. Increasing amount of cement widens throat distribution and lessens throat size. Frequency of blocked throats (inscribed radii $<10^{-4}$) not shown. Percentage of cement corresponds to the value of a, which determines cement thickness as a linear function of grain size (see text). The smallest throats not shown

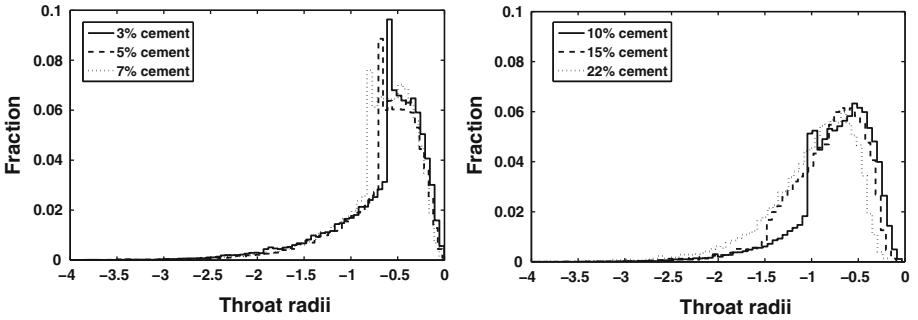

Fig. 10 Throat-size distribution (R_inscribed, logarithm values) for selected ductile-grain model rocks. All packings have 40 % ductile material with 0.7 rigid radii and different amounts of cementation. Increasing amount of cement widens throat distribution and diminishes throat size. Frequency of blocked throats not shown. Percentage of cement corresponds to the value of a, which determines cement thickness as a linear function of grain size (see text). Smallest throats not shown

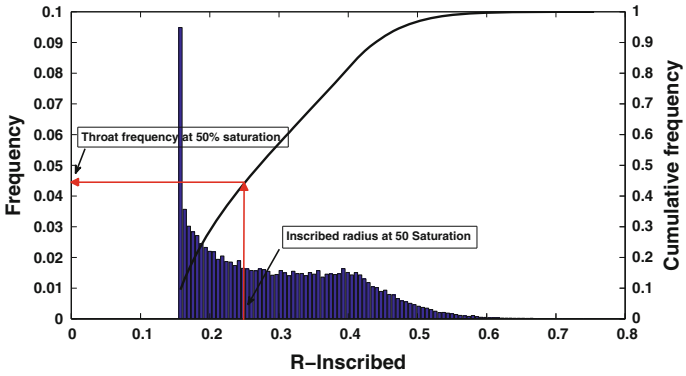

Fig. 11 Inscribed radius histogram and cumulative distribution curve for monodispersed model sediment. Inscribed radius at 50 % saturation is marked in this figure to calculate bond-percolation threshold. Bond-percolation threshold is 1—cumulative frequency of the size of the throats invaded at 50 % saturation. The latter quantity is obtained from Eq. 3

in Figs. 8 and 11. Thus for cement thicknesses less than $0.15r_i$, these model rocks have a hybrid behavior. Drainage into the throats between rigid grains will exhibit percolation, just as in the cemented packings on only rigid grains, but this percolation will be restricted to the subnetwork of pores connected by such throats.

To see this, compare the curves for 5 % cement in Figs. 4 and 5. For the rigid grain model rock, Fig. 5, the percolation threshold occurs at a dimensionless curvature of about 15 and spans essentially the entire saturation range. For the ductile grain model rock, Fig. 6, the percolation threshold occurs at a larger dimensionless curvature (about 25) even though the large pore throats are the same size as in the rigid grain model. This is because the ductile grain model has smaller connectivity. When percolation occurs, it spans less of the saturation range than for the rigid-grain model. This is because the blocked and very small throats control access to a significant volume of the pore space. The wetting phase in this volume becomes disconnected from the outlet during percolation of the non-wetting phase, forming a large irreducible wetting phase saturation of 30 % in the ductile grain model.

By the time the cement thickness is large enough (i.e., $>0.10r_i$) to start closing throats between rigid grains in the ductile-grain model, the pore space connectivity is already small. Thus, the gradual shift of drainage curves upward and rightward in Fig. 5 is compressed to a very small region in Fig. 6, and the behavior is dominated by the large fraction of isolated pores.

8 Percolation Threshold for Pore Space in Tight-Gas-Sand Models

In networks with all throats open, the percolation threshold is obvious (cf. curves for greater than 15 % porosity in Fig. 5). In networks with some fraction of throats closed, the existence of a spanning cluster of drained pores can be harder to discern, as it may emerge gradually in a simulation in a finite network like those used here. Thus, we estimate the bond-percolation threshold from capillary-pressure drainage curves heuristically by assuming that a 50 % saturation of the non-wetting phase spans the network. This will be true and will introduce little error for drainage simulations in networks with all throats open. It may not be true for networks with a large fraction of closed throats, but the heuristic does give a common and very easily calculated basis for comparing the behavior between models. At percolation, the gas-phase permeability should be significant. If no percolation is present at 50 % wetting-phase saturation, production from the reservoir may not be economical. The choice of saturation for this heuristic could thus be adjusted to account for gas prices, production costs, etc.

The dimensionless curvature at which 50 % saturation is reached during drainage is easily observed. The inscribed radius corresponding to this curvature is:

$$R_{\text{inscribed}} = \left(\frac{2}{\text{Curvature} + 1.6}\right) \times R_{\text{mean}} \tag{3}$$

where $R_{\text{inscribed}}$ is the inscribed radii, R_{mean} the mean radius of hard grains, and Curvature is the curvature at 50 % saturation.

The location of this particular value on the cumulative frequency distribution of throat sizes gives an estimate of how many of the throats could have been drained at this saturation (Fig. 11). That is, if all throats had access to the non-wetting phase, then all throats larger than the inscribed radius calculated in Eq. 3 would have drained. Not all throats have access to the non-wetting phase, but this assumption enables an easy assessment of the trends. The bond-percolation threshold is the fraction of throats drained when the spanning cluster first forms, so it is given by one minus the cumulative throat frequency at the calculated inscribed radius.

Figure 12 shows the bond-percolation threshold estimated in this way for both rigid-grain and ductile-grain models with different amounts of cementation. When the rigid-model rock has no cement, all of the throats are open and the estimated percolation threshold is 55 %. This agrees fairly well with the more rigorous estimate of 50 % (Mellor 1989; Bryant et al. 1996). Addition of 0.05–$0.10r_i$ cement (5–10 % of sphere radii added to the sphere) to this packing does not increase the percolation threshold because the fraction of blocked throats does not change. Adding cement beyond $0.10r_i$ of sphere radius reduces open throats (increases blocked throats) in the model rock and increases the percolation threshold. The model rocks with less than 5 % porosity have estimated thresholds exceeding 80 %. This suggests that effective gas permeability can be quite small even at large gas saturations in such rocks.

The percolation thresholds estimated for the ductile-grain model rocks are shown also in Fig. 12. Adding cement (up to $0.10r_i$) increased the bond-percolation threshold from 0.63 to

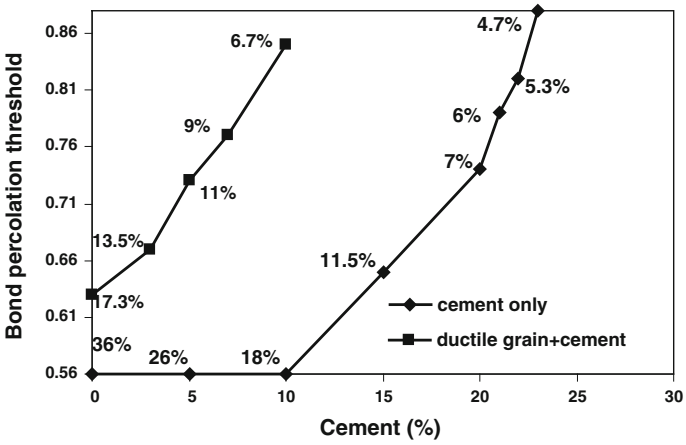

Fig. 12 Bond-percolation threshold and fraction of blocked throats for both rigid-grain and ductile-grain dominated model rocks with different cementations. Percentages on top of data show porosity percentage for each packing

0.85. Thus, the undesirable situation of having small effective gas permeability at large gas saturations would be encountered at larger porosities in this class of rocks.

9 Comparison Between Drainage Simulation and Experimental Data

To compare simulated drainage curves to experimental data, the dimensionless curvatures were converted to capillary-pressure using the mean grain radius of the sample and the interfacial tension for the fluids used in the experiment:

$$P_c = \frac{C \times \sigma \times 10^{-4}}{R_{mean}} \tag{4}$$

where P_c is capillary pressure (KPa), σ is interfacial tension between air and mercury (which is 484 dynes/cm or mN/m), R_{mean} is the mean grain radius of the sample in (m), and C is the curvature derived from simulation. In these units, the equation should be written as:

$$P_c = \frac{C \times 484}{R_{mean}} \tag{5}$$

A sample of tight gas sandstone from Piceance formation at the depth of 4,578 ft. (www.discovery-group.com) with 3.95 % porosity and less than 5 % ductile grains was selected. A rigid-grain model with $0.24r_i$ cement (4.1 % porosity) was selected to compare with lab data. The radius of the model sediment grains was set to 175 μm to match the grain size of rock sample. The model gives a good prediction of the laboratory drainage curve, including the absence of percolation (Fig. 13a).

The drainage curve for a ductile-grain model with $0.15r_i$ cement, 40 % ductile grains and 3.6 % porosity agrees well with measurement on a sample from the Green River Formation at a depth of 12,520 ft. (www.discovery-group.com), with mean grain radii of 175 µm, 38 % ductile grains and porosity of 4 %, as in Fig. 13b. The data are consistent with the predicted effect of ductile grains on the drainage curve, namely the steepening of the curve (large magnitude of dP_c/dS_w) at large S_w,

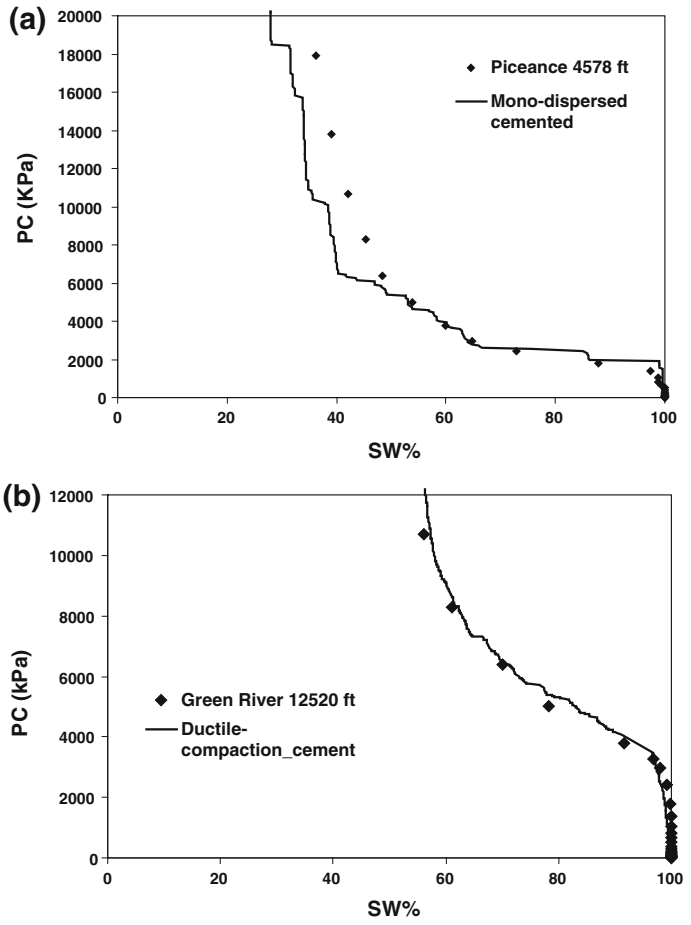

Fig. 13 **a** Comparison of drainage curves between rigid-grain dominated model rock and lab measurement (data courtesy of www.discovery-group.com). Model rock is very well sorted with $0.24r_i$ cement, 175 micron grains and porosity = 4.1 %. Porosity for tight-gas sample is 3.95 %, and grain size is 175 micron. Sample rock shows little microporosity, less than 5 % ductile grain, and void space is mainly intergranular (Data courtesy of www.discovery-group.com). **b** Simulated drainage curves using a ductile-grain model rock (40 % moderately ductile grains) and cement thickness of $0.15r_i$. Porosity for this sample is 3.6 %. Lab sample from Green River Formation (depth = 12,520 ft.), with mean grain radius of 175 μm and porosity = 4 %. This sample rock shows little microporosity, and void space is mainly intergranular (Data courtesy of www.discovery-group.com)

We have good agreement with the sample rocks because these tight-gas samples have no depositional matrix and microporosity is sparse. The approach described here cannot explain drainage curves in rocks with a good deal of microporosity in their textures (Mousavi 2010). Multiscale networks are a promising method for such rocks (Sakhaee-Pour 2012; Mehmani et al. 2011).

10 Conclusion

Grain-scale simulation of porosity-reducing mechanisms in tight-gas sandstones (ductile-grain deformation, cement precipitation) shows that pore space is poorly connected in these

rocks. Ductile grain content and cement reduce connectivity rapidly for porosities below 10 %. The calculated percolation threshold at 50 % saturation of the wetting phase for these low-porosity packings is large, meaning a large fraction of throats and pores must be drained to achieve 50 % saturation of the gas phase. The drainage curves are sensitive to the presence of ductile grains and amount of cementation for model rocks with less than 10 % porosity. Compaction and cementation change the shape of drainage curves in different ways because they influence the throat-size distributions differently. The predicted drainage curves for the rigid-grain and ductile-grain models agree with measurements in tight-gas sandstones with little or no microporosity.

Acknowledgments The authors thank and acknowledge Cynthia Thane and Javad Behseresht for permission to use their program for simulations. Publication authorized by the Director, Bureau of Economic Geology.

References

Al-Raoush, R., Thompson, K.E., Clinton, S.W.: Comparison of network generation techniques for unconsolidated porous media. Soil Sci. Soc. Am. J. **67**(6), 1687–1700 (2003)

Behseresht, J.: Infinite acting physically representative networks for capillary-controlled displacements. A thesis submitted to Department of Petroleum Engineering and Geosystems of University of Texas at Austin in partial fulfillment of Master of Science in Engineering (2008)

Behseresht, J., Bryant, S.L.: Sedimentological control on saturation distribution in Arctic gas-hydratebearing sands. Fire in the Ice **11**(1), 10–12 (2011)

Behseresht, J., Peng, Y., Prodanovic, M., Bryant, S.L.: Grain scale study of hydrate formation in sediments from methane gas: role of capillarity. In: Proceedings of the 6th International Conference on Gas Hydrates, Vancouver, BC, Canada (2008)

Behseresht, J., Bryant, S.L., Sepehrnoori, K.: Infinite-acting physically representative networks for capillary-controlled displacements. SPE J. **14**(4), 568–578 (2009)

Bryant, S.L., Mason, G., Mellor, D.: Quantification of spatial correlation in porous media and its effect on mercury porosimetry. J. Colloid Interface. Sci. **177**, 88–100 (1996)

Bryant, S.L., Cade, C., Mellor, D.: Permeability prediction from geologic models. AAPG Bull. **77**(8), 1338–1350 (1993)

Bourbie, T., Zinszner, B.: Hydraulic and acoustic properties as a function of porosity in fontainebleau sandstone. J. Geophys. Res. **90**, 11524–11532 (1985)

Dutton, S.P., Clift, S.J., Hamilton, D.S., Hamlin, H.S., Hentz, T.F., Howard, W.E., Akhter, M.S., Laubach, S.E.: Major low-permeability sandstone gas reservoirs in the continental United States (Report of Investigations No. 211). University of Texas at Austin, Bureau of Economic Geology (1993)

Finney, J.: Random packing and the structure of the liquid state. A dissertation submitted to Department of Earth Sciences of University of London in partial fulfillment of the requirements for the degree of Doctor of Philosophy (1968)

Fisher, R.A.: On the capillary forces in an ideal soil; correction of formulae given by W.B. Haines. J. Agric. Sci. **16**, 492–505 (1962)

Gladkikh, M., Bryant, S.: Prediction of imbibitions in unconsolidated granular materials. J. Colloid Interface Sci. **288**, 526–539 (2005)

Haines, W.B.: Studies in the physical properties of soil. V. The hysteresis effects in capillary properties and the modes of moisture distribution associated therewith. J. Agric. Sci. **20**, 97–116 (1930)

Houseknecht, D.W.: Influence of grain size and temperature on intergranular pressure solution, quartz cementation and porosity in a quartzose sandstone. J. Sed. Petrol. **54**(2), 348–361 (1984)

Jin, G., Patzek, T.W., and Silin, D.B.: Modeling the impact of rock formation history on an evolution of absolute permeability. In: SPE annual technical conference and exhibition, Houston, TX (2006)

Joekar-Niasar, V., Prodanović, M., Wildenschild, D., Hassanizadeh, S.M.: Network model investigation of interfacial area, capillary pressure and saturation relationships in granular porous media. Water Resour. Res. **46**, W06526 (2010)

Mason, G.: Desaturation of porous media. I. Unconsolidated materials. J. Colloid Interface Sci. **41**(2), 208–227 (1972)

Mason, G., Mellor, D.W.: Simulation of drainage and imbibitions in a random packing of equal spheres. J. Colloid Interface Sci. **176**, 214–225 (1995)

Mehmani, A., Tokan-Lawal, A., Prodanović, M., Sheppard, A. P.: The effect of microporosity on transport properties in tight reservoirs. In: SPE unconventional gas conference, Woodlands, TX (2011)

Mellor, D.W.: Random close packing (RCP) of equal spheres: structure and implications for use as a model porous medium. A dissertation submitted to Department of Earth Sciences of Open University, United kingdom in partial fulfillment of the requirements for the degree of Doctor of Philosophy (1989)

Milliken, K.L., Choh, S.-J., McBride, E.F.: Sandstone Petrology, v. 2.0, A Tutorial Petrographic Image Atlas, Multimedia CD-ROM: American Association of Petroleum Geologists/DataPages, Discovery Series No. 10 (Second Edition), Tulsa, Oklahoma, CD-ROM (2007)

Mousavi, M.A., Bryant, S.L.: Geometric models of porosity reduction by ductile grain compaction and cementation. AAPG Bull., submitted (2011)

Mousavi, M.A.: Pore scale characterization and modeling of two-phase flow in tight gas sandstones. A dissertation submitted to Department of Petroleum Engineering and Geosystems of University of Texas at Austin in partial fulfillment of the requirements for the degree of Doctor of Philosophy (2010)

Mousavi, M.A., Bryant, S.L.: Geometric models of porosity reduction mechanisms in tight gas sands. In: SPE rocky mountain oil and gas technology symposium, Denver, CO (2007)

Roberts, J.N., Schwartz, L.M.: Grain consolidation and electrical conductivity in porous media. Phys. Rev. B. **31**(9), 5990–5997 (1985)

Sakhaee-Pour, A.: Gas flow through shale. A dissertation submitted to Department of Petroleum Engineering and Geosystems of University of Texas at Austin in partial fulfillment of the requirements for the degree of Doctor of Philosophy (2012)

Thane, C.G.: Geometry and topology of model sediments and their influence on sediment properties. A thesis submitted to Department of Petroleum Engineering and Geosystems of University of Texas at Austin in partial fulfillment of Master of Science in Engineering (2006)

Valvatne, P.H., Blunt, M.J.: Predictive pore-scale network modeling of two phase flow in mixed wet media. Water Resour. Res. **40**, W07406 (2004)

Worden, R.H., Morad, S.: Quartz Cementation in Sandstones. International Association of Sedimentologists Special Publications 29. Blackwells, Oxford (2000)